Electron thermal transport within magnetic islands in the reversed-field pinch[a)]

H. D. Stephens,[1,b)] D. J. Den Hartog,[1,3] C. C. Hegna,[1,2] and J. A. Reusch[1]
[1]*Department of Physics, University of Wisconsin–Madison, 1150 University Ave., Madison, Wisconsin 53706, USA*
[2]*Department of Engineering Physics, University of Wisconsin-Madison, 1500 Engineering Drive, Madison, Wisconsin 53706, USA*
[3]*Center for Magnetic Self-Organization in Laboratory and Astrophysical Plasmas, University of Wisconsin–Madison, Madison, Wisconsin 53706, USA*

(Received 20 November 2009; accepted 22 March 2010; published online 3 May 2010)

Tearing mode induced magnetic islands have a significant impact on the thermal characteristics of magnetically confined plasmas such as those in the reversed-field pinch (RFP). New Thomson scattering diagnostic capability on the Madison Symmetric Torus (MST) RFP has enabled measurement of the thermal transport characteristics of islands. Electron temperature (T_e) profiles can now be acquired at 25 kHz, sufficient to measure the effect of an island on the profile as the island rotates by the measurement point. In standard MST plasmas with a spectrum of unstable tearing modes, remnant islands are present in the core between sawtoothlike reconnection events. Associated with these island remnants is flattening of the T_e profile inside the island separatricies. This flattening is characteristic of rapid parallel heat conduction along helical magnetic field lines. In striking contrast, a temperature gradient within an $m=1$, $n=5$ island is observed in these same plasmas just after a sawtooth event when the $m=1$, $n=5$ mode may briefly come into resonance near the magnetic axis. This suggests local heating and relatively good confinement within the island. Local power balance calculations suggest reduced thermal transport within this island relative to the confinement properties of standard MST discharges between reconnection events. The magnetic field and island structure is modeled with three-dimensional nonlinear resistive magnetohydrodynamic simulations (DEBS code) with Lundquist numbers matching those in MST during standard discharges. During improved confinement plasmas with reduced tearing mode activity, temperature fluctuations correlated with magnetic signals are small with characteristic fluctuation amplitudes of order $\tilde{T}_e/T_e \sim 2\%$. © *2010 American Institute of Physics*.
[doi:10.1063/1.3388374]

I. INTRODUCTION

The Madison Symmetric Torus[1] (MST) reversed-field pinch (RFP) is a toroidal magnetic confinement device with a major radius, R, of 1.5 m and a minor radius, r, of 0.52 m. The magnetic field is characterized by toroidal components (B_ϕ) in the core and edge that are oppositely directed and poloidal field (B_θ) which is of the same order of magnitude as the toroidal field. In conventional operation of the MST many unstable tearing modes[2] are resonant. Owing to the rapid equilibration processes along field lines in high temperature plasmas, magnetic islands which connect field lines at smaller radii to field lines at larger radii tend to locally flatten the electron temperature profile within the island separatrices.[3–9] Tearing instabilities in the RFP are often sufficiently virulent that the magnetic islands overlap. Overlapping islands begin to form large scale stochastic fields increasing the radial scale length of heat transport. However, recent improvements in the MST Thomson scattering diagnostic have uncovered evidence of nonoverlapping magnetic islands in a variety of scenarios. Understanding the link between heat transport and remnant magnetic islands formed by these tearing modes may be key to understanding and improving confinement in the RFP. Measurement of transport in three-dimensional (3D) magnetic structures is key to understanding the self-organized helical equilibrium observed in other RFPs (Refs. 10 and 11) in which one large island reorganizes the central magnetic field topology.

This paper investigates electron thermal transport in magnetic islands in the RFP for three distinct cases. The first two cases take place in standard MST discharges with plasma currents ~400 kA and electron densities $\sim 10^{13}$ m^{-3}. Typical time traces of the plasma current and the reversal parameter, $F=B_\phi(a)/\langle B_\phi \rangle$, are shown in Fig. 1. Standard discharges in MST last between 50 and 80 ms with a flat top region in the current ~20 ms long. Discrete reconnection events called sawteeth[12] (described below in Sec. II) occur every 6–10 ms throughout the flat top region and can be seen as spikes in the reversal parameter in Fig. 1(b). In the first case (Sec. IV A), the core resonant $m=1$, $n=6$ mode (where m and n are the poloidal and toroidal wavenumbers, respectively) is investigated, first in between sawteeth and then through a sawtooth event. In standard MST plasmas between sawteeth, this mode has the largest magnetic signal and has a resonant surface that is closest to the magnetic

[a)]Paper GI3 4, Bull. Am. Phys. Soc. **54**, 95 (2009).
[b)]Invited speaker. Electronic mail: hillary@physics.wisc.edu.

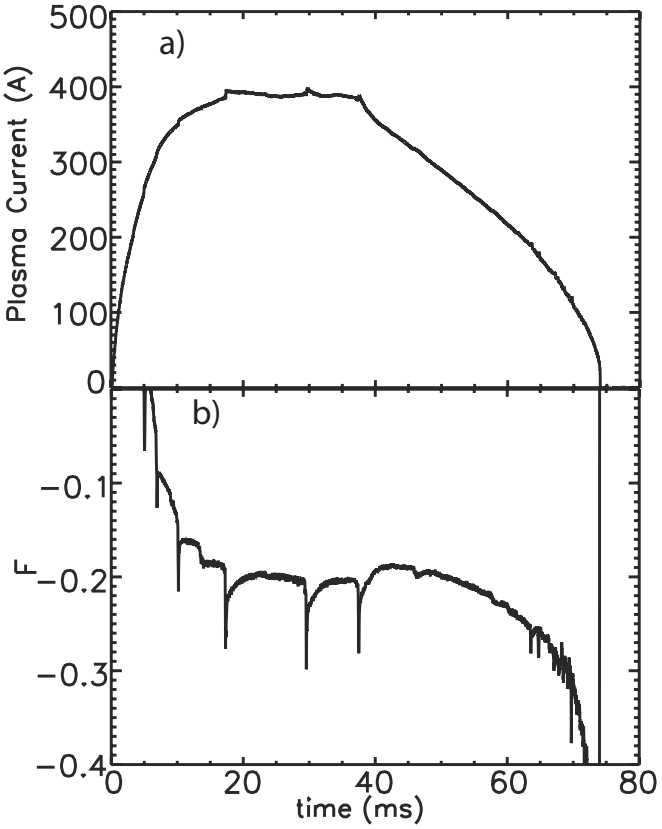

FIG. 1. Typical time traces during a standard 400 kA MST discharge for (a) the plasma current and (b) the reversal parameter, $F=B_\phi(a)/\langle B_\phi\rangle$ Note the sharp downward spikes associated with sawteeth.

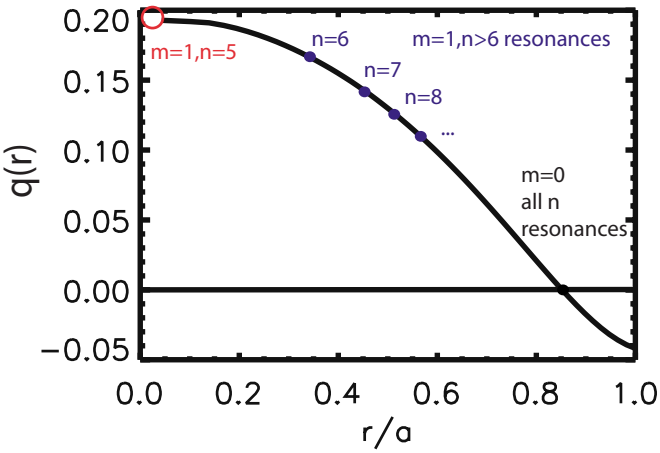

FIG. 2. (Color online) The safety factor, q, peaks on axis at a value of ~ 0.2 and goes through zero near the edge at the reversal surface. Tearing modes are resonant at rational values of q. For all discharges studied in this work, $m=1$, $n\geq 6$ and all $m=0$ modes are always resonant in the plasma. The q-profile evolves during a sawtooth event and has a peak $q(0)>0.2$ at the crash at which point the $m=1$, $n=5$ mode (open circle) becomes resonant.

axis. This mode partially, but not completely, overlaps with the $m=1$, $n=7$ mode, and maintains a remnant island structure throughout much of its evolution. Electron temperature measurements correlated with this $m=1$, $n=6$ magnetic tearing mode show a helical flattening of the electron temperature profile in the presence of this remnant island between sawteeth. The remnant island and the associated electron temperature structure disappear during discrete sawtooth events when mode amplitudes spike. In the second case (Sec. IV B), a $m=1$, $n=5$ mode present near the magnetic axis just after a sawtooth, is studied. Remarkably, the appearance of a helically peaked temperature profile is observed indicating transient good confinement near the magnetic axis following a sawtooth. The third case (Sec. IV C) involves nonstandard, sawtooth-free, improved-confinement discharges where the overall amplitude of magnetic fluctuations has been reduced. In this final case it is seen that correlated electron temperature fluctuations are small when magnetic fluctuations are small (Sec. IV C).

The remainder of this paper is organized as follows. Section II gives some background on the magnetic tearing modes present in MST. Section III describes how the correlation between magnetic fluctuations and temperature fluctuations is performed. Results are presented in Sec. IV followed by a discussion in Sec. V.

II. TEARING MODES IN MST

The equilibrium configuration of the RFP is characterized by a toroidal magnetic field that reverses direction in the edge relative to the toroidal field on axis. This results in a safety factor profile, $q(r)=(rB_\phi)/(RB_\theta)$, that passes through zero and reverses direction. See Fig. 2 for a typical q-profile. In standard MST discharges the highest value of q is on axis with $q(0)\lesssim 0.2$. Tearing modes are resonant where $\vec{k}\cdot\vec{B}=0$, which occurs where q takes on rational values of m/n (where m and n are the poloidal and toroidal wavenumbers, respectively). In MST, several low wavenumber modes are resonant. Specifically, the $m=1$, $n\geq 6$ modes are always resonant inside the reversal surface and all $m=0$ modes are resonant, where $q=0$. Outside the reversal surface $m=1$ modes with negative n values are present; the specific modes depend on how deeply the field is reversed. The $m=1$, $n=6$ mode is usually the core-most resonant mode and the largest amplitude mode. However if $q(0)$ reaches 0.2, the $m=1$, $n=5$ mode becomes resonant. Equilibrium reconstructions performed using MSTFIT,[13] a nonlinear Grad–Shafranov toroidal equilibrium reconstruction code, show that for the plasmas discussed in this paper $q(0)<0.2$ except for during a sawtooth event (described below) when it may jump above 0.2 for ~ 1 ms.

The peaked parallel current density profile in the RFP provides a free energy source for tearing modes to grow and form magnetic islands. As the islands grow they overlap with neighboring modes resulting in a field that is mostly stochastic. The rational surfaces of modes resonant in the core are spaced farther apart than modes resonant further out. The $m=1$, $n=6$ mode does not fully overlap with the neighboring $n=7$ and a remnant island structure is present. Simulations have been performed at realistic Lundquist numbers ($S\sim 3.8\times 10^6$) using the 3D resistive magnetohydrodynamic (MHD) DEBS code.[14] In order to see this remnant island structure visually the magnetic fields produced by the DEBS

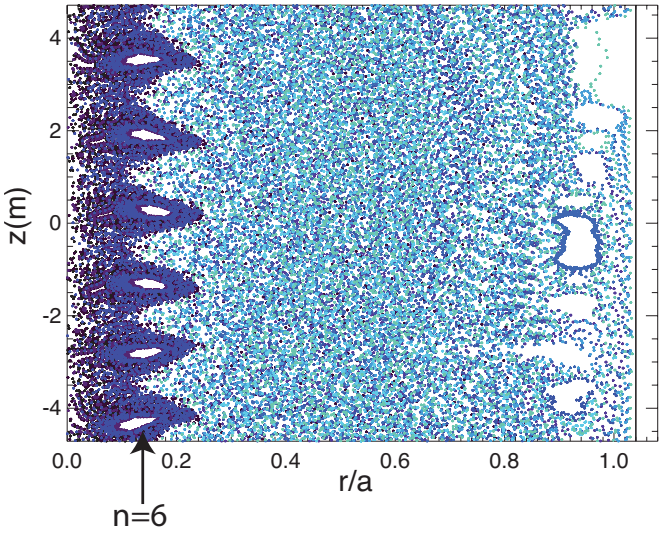

FIG. 3. (Color) Magnetic field line tracing performed by the MAL code (Ref. 15) with results of DEBS (Ref. 14) simulations in between sawtooth crashes. A remnant $m=1$, $n=6$ island is visible at $r/a \sim 0.15$ m.

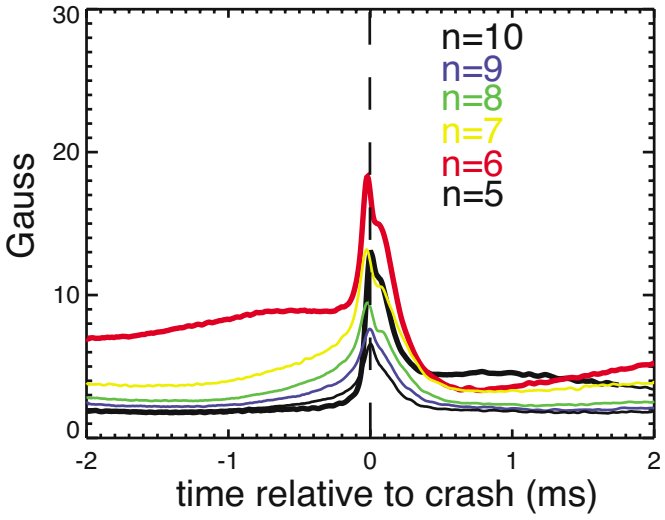

FIG. 4. (Color online) An ensemble of $m=1$, $n=5-10$ magnetic fluctuation data through a sawtooth crash. The $n=6$ fluctuation is the largest mode before the crash. The $n=5$ fluctuation is almost zero before the sawtooth crash and is briefly the largest mode after the crash.

code, scaled such that the toroidal flux matches the toroidal flux measured in MST, are mapped by the field line tracing code MAgnetic Lines (MAL).[15] Figure 3 shows the results of this process for a simulation of a standard plasma. The simulation exhibits quasiperiodic burst of tearing mode growth similar to the sawtooth events observed in the experiment. The results in Fig. 3 reflect the magnetic field structure between sawteeth. A clear $m=1$, $n=6$ remnant island structure is visible in the plasma core.

During simulated sawteeth the amplitude of the magnetic tearing fluctuations spike, the $m=1$, $n=6$ and $m=1$, $n=7$ modes completely overlap, the magnetic field shown in Fig. 3 becomes completely stochastic and the remnant island structure disappears. Experimentally, tearing mode activity from sawtooth to sawtooth and from one plasma discharge to the next is very reproducible so that data collected from several different sawteeth and plasma discharges can be ensembled to gain a clear picture of phenomena associated with the sawtooth. Figure 4 shows the amplitude of several magnetic tearing fluctuations through a sawtooth crash for an ensemble of data. The $n=6$ is the largest mode for most of the plasma duration and has a rational surface that is the core-most resonant. Before the sawtooth crash the $m=1$, $n=6$ tearing mode has the largest amplitude. During the sawtooth crash the $m=1$, $n=5$ mode briefly comes into resonance. Just after the sawtooth crash the $m=1$, $n=5$ mode is the largest and core most mode. It is of particular interest because of its proximity to the axis. When it is present, it dominates the mode activity in the core. This paper deals with temperature fluctuations associated with the $m=1$, $n=6$ tearing mode between sawteeth and during a sawtooth event, and $m=1$, $n=5$ tearing modes just after a sawtooth crash when the $m=1$, $n=5$ mode has the largest amplitude in the magnetic spectrum.

III. MAPPING ELECTRON TEMPERATURE TO TEARING MODES

The Thomson scattering diagnostic on MST (Refs. 16–18) has recently been upgraded[19] to have burst mode capability (6 pulses at 25 kHz every 1 ms) enabling opportunities to study fast electron temperature dynamics. The Thomson scattering diagnostic measures electron temperature at 21 spatial locations (resolution $\lesssim 2$ cm) vertically from the core of MST down to the bottom edge. Magnetic islands formed by tearing modes rotate in both the poloidal and toroidal directions past the diagnostic at approximately 10–20 kHz. The exact position of the mode as it rotates past is measured with magnetic coil arrays. As time passes the diagnostic samples different parts of the island and a temporally resolved measurement can be translated into a spatially resolved measurement. The electron temperature at a given radial location as a function of a given mode's position can be modeled as

$$T_e = T_{e0} + \tilde{T}_{e,n} \cos(\theta_n). \quad (1)$$

Here, T_e is the measured electron temperature data and θ_n is the poloidal position of the O-point for a given mode at the Thomson scattering diagnostic toroidal location. The model parameters are T_{e0}, the mean electron temperature and $\tilde{T}_{e,n}$, the fluctuation amplitude. Only fluctuations associated with one mode can be tested at a time. Any fluctuations not correlated with the mode of interest average to zero over a large enough ensemble. Bayesian probability theory[20] is utilized to ensemble the data.

Bayesian probability theory is based on two simple rules of basic probability theory. The product rule

$$P(X,Y|I) = P(X|Y,I)P(Y|I) \quad (2)$$

which reads, "The probability that specific values of X and Y are true values given background information, I, is equal to

the probability that X is the true value given Y and I, times the probability that Y is the true value given background information." The second rule is the sum rule

$$P(X|I) + P(\bar{X}|I) = 1, \tag{3}$$

where $\bar{X}$ means that "X is not true."

The basic idea behind Bayesian analysis is that the probability that a given parameter, X, is true given all the data, d, uncertainty, σ, and any relevant background information, I, $P(X|d,\sigma,I)$, can be found by calculating three other easier to obtain quantities. These are the likelihood probability distribution function (PDF), $P(d|X,\sigma,I)$, the probability of getting the data given X, the prior PDF, $P(X|I)$, the probability of measuring X given relevant background information (e.g., temperature cannot be a negative number) and the evidence, $P(d|I)$, a normalization factor.

$$P(X|d,\sigma,I) = \frac{P(d|X,\sigma,I)P(X|I)}{P(d|I)}. \tag{4}$$

Equation (4) is called Bayes Theorem and follows directly from the product rule [Eq. (2)]. Bayes Theorem sets up a framework in which the unknowns can be calculated in terms of the knowns in a straightforward way. Another useful corollary of probability theory is marginalization, which allows the probability calculation for interesting quantities while getting rid of the dependence on uninteresting quantities or nuisance parameters. This is advantageous because the calculation can be done with out assuming the value of the nuisance parameter is known. The marginalization procedure is defined as

$$P(X|I) = \int_{-\infty}^{\infty} P(X,Y|I)dY. \tag{5}$$

Because Bayesian analysis returns the entire PDF no information has been lost. As more data are gathered more information is added to the final PDF and a true representation of the answer would be to display the entire PDF. However, since we are used to thinking in terms of a best fit value plus error bars, the value with the maximum probability is synonymous to the best fit and the points at which the PDF drops to $1/e$ of its maximum synonymous to the error bars.

In the case of electron temperature fluctuation analysis Bayes Theorem tells us that

$$P(\tilde{T}_{e,n}, T_{e0}|T_{e_A}, T_{e_B} I) \propto P(T_{e_A}|\tilde{T}_{e,n}, T_{e0}, I)P(T_{e_B}|\tilde{T}_{e,n}, T_{e0}, I)P(\tilde{T}_{e,n}, T_{e0}|I). \tag{6}$$

Here, T_{e_A} and T_{e_B} (or generally T_{e_i}) are electron temperature measurements taken in quick succession. At least two temperature measurements must be used and the Thomson scattering diagnostic provides up to six in a burst. We assume a Gaussian probability distribution for the electron temperature measurement and can calculate the likelihood PDF.

$$P(T_{e_i}|\tilde{T}_{e,n}, T_{e0}, I) = \frac{\exp\left(-\frac{1}{2}\chi_i^2\right)}{\sigma_i\sqrt{2\pi}}, \tag{7}$$

$$\chi_i^2 = \left[\frac{T_{e,\text{measured},i} - T_{e,\text{expected},i}(\tilde{T}_{e,n}, T_{e0}, \theta_{n,i})}{\sigma_i}\right]^2. \tag{8}$$

The prior PDF, $P(\tilde{T}_{e,n}, T_{e0}|I)$, is taken to be constant over a range of physically reasonable values. With this the right hand side of Eq. (6) can be evaluated.

Equation (6) does not find the distribution of values of $\tilde{T}_e$ and T_{e0} rather it finds the probability that specific combinations of $\tilde{T}_e$ and T_{e0} are true. The difference between Bayesian probability theory and orthodox statistics is highlighted here, although it may be subtle. Bayesian probability theory is chosen here because it is impossible to measure with no uncertainty the values of $\tilde{T}_e$ and T_{e0} each shot. In essence the question is not what is the distribution of $\tilde{T}_e$ and T_{e0}, but rather what is the true value of $\tilde{T}_e$ and T_{e0}. In order to do this the assumption must be made that there is a true value. At any given time this is certainly the case, however the plasma system is dynamic and there may be shot-to-shot variation (or even burst-to-burst variation—variation in plasma conditions from one burst of laser pulses to the next in the same plasma shot). Because of this, data chosen to ensemble together have tight constraints to ensure that the true value of $\tilde{T}_e$ and T_{e0} are very close for all data points in the ensemble. For results discussed in this paper this includes binning data relative to the sawtooth crash.

Shot to shot variation in T_{e0} is on the order of the expected value of $\tilde{T}_{e,n}$. In order to find $\tilde{T}_{e,n}$ it is assumed that $\tilde{T}_{e,n}$ is constant shot to shot, but T_{e0} is not necessarily constant. Thus, $\tilde{T}_{e,n}$ becomes the interesting quantity and T_{e0} a nuisance parameter which is marginalized out. The probability for a single burst of laser pulses is marginalized with respect to T_{e0} and the PDF becomes a function of $\tilde{T}_{e,n}$ alone.

$$P(\tilde{T}_{e,n}|T_{e_A}, T_{e_B}, I) = \int P(\tilde{T}_{e,n}, T_{e0}|T_{e_A}, T_{e_B}, I)dT_{e0}. \tag{9}$$

Once the marginalized PDF for one burst of laser pulses has been found, the product rule is used to combine data from all shots.

$$P(\tilde{T}_{e,n}|T_{e_{\text{all}}}, I) = \prod_i^{\text{shots}} P(\tilde{T}_{e,n}|T_{e_{A_i}}, T_{e_{B_i}}, I). \tag{10}$$

Figure 5 shows how the PDF of Eq. (10) collapses down to a narrow range of possible values for $\tilde{T}_{e,6}$ as information from additional MST shots is added to the ensemble.

A Monte Carlo simulation has been done to address the question of what would happen with the analysis if $\tilde{T}_{e,n}$ was not constant from shot to shot. If values change from shot to shot but have a narrow distribution then the most probable value of $\tilde{T}_{e,n}$ lies in the middle of the distribution. For example, if $\tilde{T}_{e,n}$=20 eV one shot and 30 eV the next the most probable value which is calculated using this analysis technique is 25 eV. However, if the values have a wider distribution the probability for the most likely value quickly drops to zero everywhere. For example if half of the shots from an 100 shot ensemble have $\tilde{T}_{e,n}$=−10 eV (a negative $\tilde{T}_{e,n}$ rep-

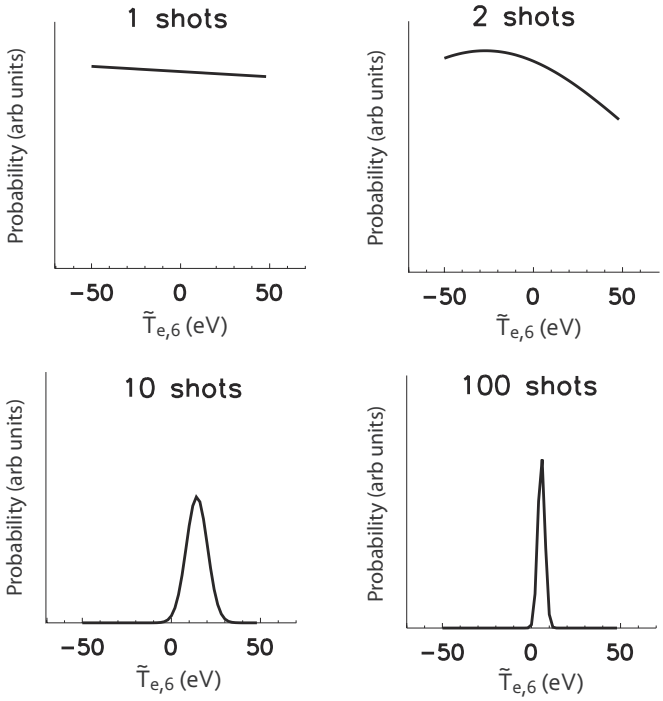

FIG. 5. The probability evolves with the data from each shot as more information is added.

resents a phase shift of π) and the other half $\tilde{T}_{e,n}$=30 eV the analysis fails to find a probable value for $\tilde{T}_{e,n}$.

In order to find T_{e0} the assumption must be made that shot-to-shot variation in the mean temperature is small. This was an assumption explicitly not made above. The PDF for T_{e0} is found is found in the same way as $\tilde{T}_{e,n}$, but with the marginalization step done with respect to $\tilde{T}_{e,n}$, treating it as a nuisance parameter and keeping T_{e0} as an interesting quantity. For data sets which are tightly constrained this appears to be a good assumption.

Two different possible scenarios for electron temperature fluctuations associated with an isolated magnetic island are sketched in Fig. 6. The first scenario details temperature signals that would be observed with an isothermal island. In general MST plasmas are hotter in the center and cooler at the edge. If an isothermal island lies somewhere between the core and the edge of the plasma it will have a temperature which lies between the temperature in the core and the edge. In this case, heating sources for the electron temperature within the island region are assumed small, rapid equilibration is assumed along the helical magnetic field lines, and slow transport processes are assumed across magnetic surfaces.[5] Electron temperature is measured along a line which extends from the center of MST down to the edge of the vacuum vessel. As the mode rotates, a single radial measurement traces out a circle which can be mapped on to a poloidal cross section Three circles are shown in the top part of Fig. 6(a). The inner, red, circle will have a higher T_{Te0} than the middle, orange circle, which will be higher than the outer, green, circle. Since the temperature within the island is lower than the temperature in the core, T_e on the red circle when the red circle is inside the island (Thomson scattering

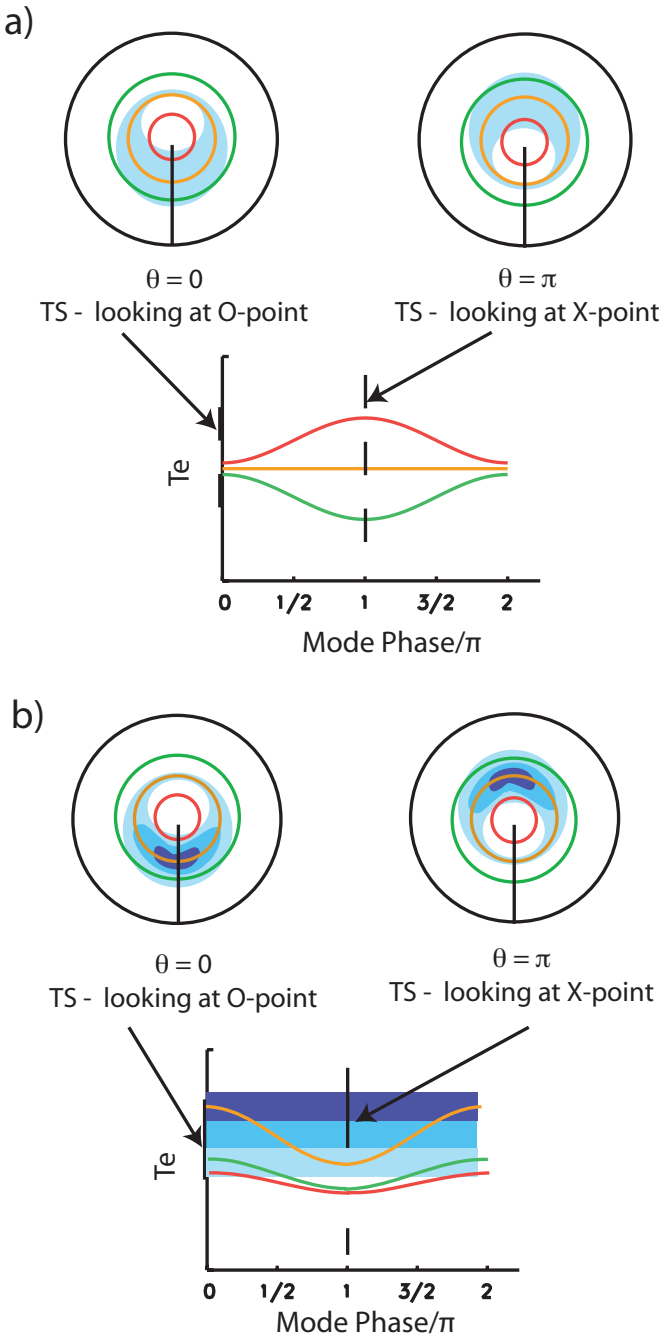

FIG. 6. (Color) Electron temperature is measured along the black vertical line from the core to the edge of MST. (a) With T_e constant inside the island (light blue): inner circle (red)—T_e is lower than circle average at O-point, middle circle (orange)—T_e is constant, outer circle (green)—T_e is higher than circle average at O-point. (b) With a T_e peak (dark blue) inside island structure: T_e fluctuations are highest for the middle circle (orange) sampling the hot spot.

diagnostic measuring temperature across the O-point) will be lower than the circle average. Similarly T_e is higher on the red circle when looking across the X-point. This means the amplitude of the temperature fluctuation, $\tilde{T}_{e,n}$, from Eq. (1) is negative. Temperature along the middle, orange, circle is constant since it is in the isothermal island and thus has $\tilde{T}_{e,n}$=0. For the outer, green, circle the temperature is higher looking across the O-point and cooler looking across the

X-point so the value of $\tilde{T}_{e,n}$ will be positive. In summary, fluctuations associated with an isothermal island structure will exhibit a phase flip (fluctuation amplitude passes through zero and reverses sign) across the center of the O-point for the mode. This is because the fluctuations on the inside of the resonant surface tend to lower the temperature and fluctuations on the outside of the resonant surface tend to raise the temperature to produce a flat temperature in the island region.

The second scenario, presented in Fig. 6(b), is for an island with a temperature peak inside of the island. In this case, flux surfaces are intact inside the remnant island structure and a heating source is present within the island separatrix. Temperature fluctuations on all three circles are positive; no phase flip is observed. The temperature is always hotter across the O-point than the X-point and the largest fluctuation corresponds to the radial location that samples the hot spot. Estimates for the cross field heat transport within the magnetic island can be made.

IV. RESULTS

Electron temperature fluctuations associated with tearing modes are studied in three cases. Each case produces different results. In the first case the electron temperature is flattened across a core remnant island (Sec. IV A). In contrast to this, the electron temperature is found to peak in relation to a mode near the magnetic axis (Sec. IV B). Finally, electron temperature fluctuations are found to be small when the magnetic tearing modes have been reduced with parallel-current profile control (Sec. IV C).

A. $m=1$, $n=6$ Isothermal Island

Electron temperature fluctuations associated with the $m=1$, $n=6$ tearing mode were studied in standard plasmas with plasma current of 400 kA $\pm$ 15% and plasma density $\sim 10^{13}/\mathrm{cm}^3$. Between sawtooth crashes (>3 ms from a sawtooth event) the observed electron temperature fluctuations are consistent with temperature flattening across the island separatrix. Figure 7(a) shows the temperature fluctuation amplitude across the minor radius of the plasma at the Thomson scattering diagnostic's measurement locations. The fluctuation amplitude is negative on the inside of the rational surface, passes through zero at the rational surface for the mode and is positive on the outside of the rational surface. This corresponds with the first scenario presented in Fig. 6. The radial location where the fluctuation amplitude reverses is clearly defined, pinpointing the location of the island separatrix. Peak to peak fluctuation levels are around 20–40 eV in a background of ~300 eV. Figure 7(b) shows the calculated electron temperature across a X-point (negative r/a values) and an O-point (positive r/a values) using Eq. (1) and the results for T_{e0} and $\tilde{T}_{e,6}$ from the Bayesian analysis described in Sec. III A clear flattening of the temperature profile across the O-point can be seen. These observations are consistent with the presence of a remnant island structure prior to the sawtooth crash and the magnetic fields not being fully stochastic.

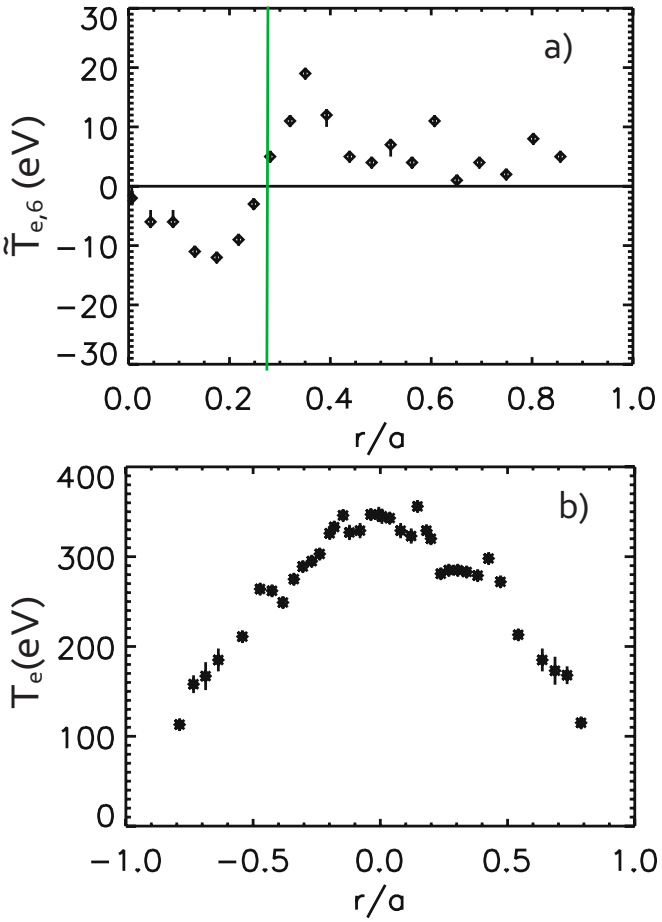

FIG. 7. (Color online) (a) Electron temperature fluctuation amplitude associated with the $m=1$, $n=6$ tearing mode between sawteeth at the radial locations measured by the Thomson scattering diagnostic. (b) Calculated electron temperature across a X-point (left side) and O-point (right side) using Eq. (1) and experimentally obtained values for T_{e0} and $\tilde{T}_{e,6}$. Temperature flattening across the O-point is consistent with the hypothesis of an isothermal island.

Evolution of electron temperature fluctuations associated with the $m=1$, $n=6$ tearing mode has also been observed through a sawtooth crash. Data are ensembled in 200 μs bins relative to the crash. Temperature fluctuations show a strong sawtooth dependence (see Fig. 8). As the tearing fluctuations peak at the sawtooth crash and the field becomes stochastic, correlated electron temperature fluctuations disappear. This reinforces the hypothesis that a remnant island structure is present between sawtooth crashes but the field becomes stochastic at the crash.

The radial position of the remnant magnetic island structure can be mapped relative to the sawtooth crash. Figure 9 shows that the position of the temperature structure associated with this mode moves outward after the crash from the broadening of the $J(r)$ profile and increase in q on axis.[21] Similarly, the 3D resistive MHD simulations also show the resonant surface for this mode further out after the crash. This trend is consistent with magnetic structures seen in Figs. 3 (before the crash) and 11 (just after the crash).

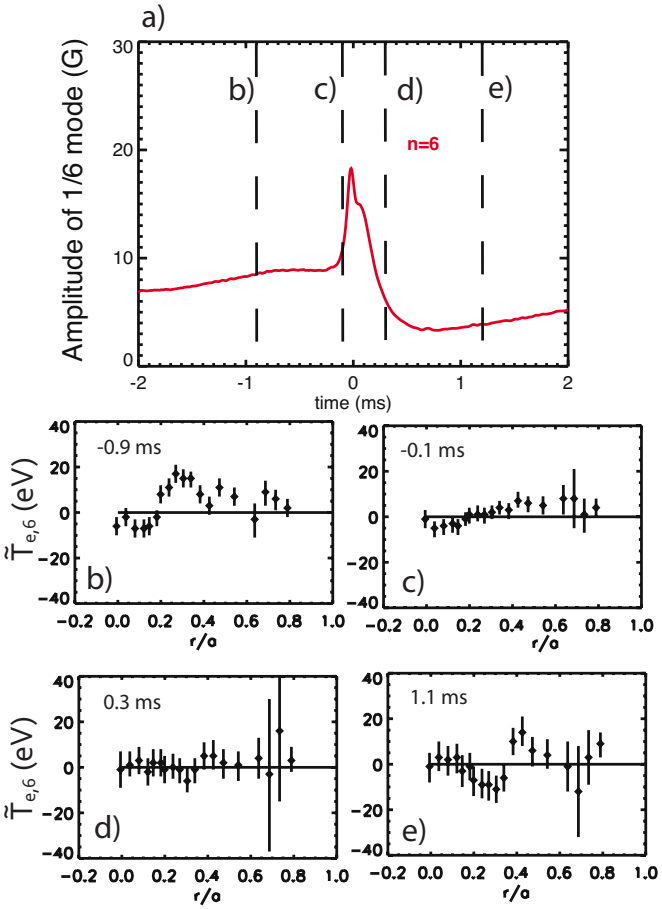

FIG. 8. (Color online) (a) Amplitude of the $m=1$, $n=6$ magnetic tearing mode relative to the sawtooth crash. Dashed lines correspond to plots (b)–(e) which are electron temperature fluctuation amplitude over the minor radius for various times. (b) Fluctuations are still large 0.9 ms before the crash. [(c)–(d)] Fluctuations correlated with $m=1$, $n=6$ tearing mode disappear at the crash. (e) Fluctuations reappear 1.1 ms after the crash.

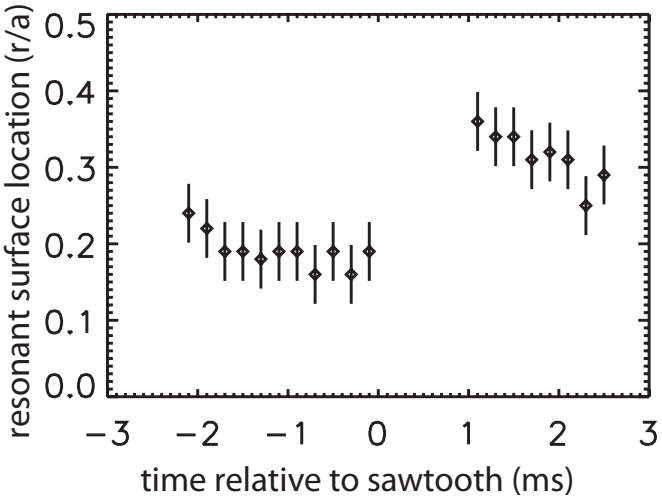

FIG. 9. Position of the $m=1$, $n=6$ zero crossing in the temperature fluctuation amplitude relative to the sawtooth crash. The remnant island structure disappears at the sawtooth crash and reappears ~1 ms later at a larger radial location.

B. $m=1$, $n=5$ helical temperature peak

Electron temperature fluctuations associated with the $n=1$, $m=5$ mode are also studied. Plasma conditions for this study are the same standard 400 kA plasmas as discussed in Sec. IV A above. For most of a plasma discharge $q(0)<0.2$ and the $n=1$, $m=5$ mode is not present in MST. During the sawtooth crash, equilibrium reconstructions using MSTFIT, show the q-profile changes so that $q(0)\gtrsim 0.2$ (with a 10% uncertainty) and the $m=1$, $n=5$ mode, which is not present before the crash, is briefly the largest mode shortly after the crash (see Fig. 4). Just after the sawtooth crash correlated fluctuations with this mode are not present, indicating the field is still stochastic as discussed above. Electron temperature fluctuations associated with this mode appear ~0.5 ms after the sawtooth crash and show a strikingly different structure than the flattening seen with the $m=1$, $n=6$ mode. The temperature fluctuations are all the same sign; there is no phase flip across a rational surface (see Fig. 10). This is consistent with the scenario presented in Fig. 6(b) showing a temperature peaking within the magnetic island. The temperature fluctuation amplitude is large compared to the background temperature (~15%) so that the temperature peak within the island is the highest temperature in the plasma. Since these fluctuations are correlated with the $m=1$, $n=5$ tearing mode this means the temperature profile peaks off the geometric axis and rotates with a $m=1$, $n=5$ helical characteristic. The peak in temperature ramps up starting at 0.5 ms after the sawtooth crash and reaches its maximum around 1.25 ms after the sawtooth crash, then begins to decay away. The length of time that the $m=1$, $n=5$ magnetic mode is large after a sawtooth crash can vary from shot to shot from ~1.5 to 4 ms so the exact sequence by which the temperature structure decays is unclear.

In addition to temperature measurements, 3D resistive MHD simulations performed at experimental values of the Lundquist number with the DEBS code have been made. These show the presence of a $m=1$, $n=5$ magnetic structure with intact magnetic flux surfaces just after the crash (see Fig. 11). These simulations also show that although the $m=1$, $n=5$ mode briefly comes into resonance after the sawtooth crash the decrease in the amplitude of the mode does not correspond directly to when the mode moves out of resonance. The amplitude of the mode and associated magnetic structure shown in Fig. 11 can be present for a few ms after the mode becomes nonresonant, suggesting that this mode maybe an ideal mode rather than a tearing mode.

C. Parallel current profile control

Magnetic tearing mode amplitudes in the RFP can be reduced by inductively controlling the parallel current profile and reducing the free energy source for these modes.[22] The $m=1$, $n=6$ fluctuation goes from ~10 G in standard plasmas to $\lesssim 3$ G in plasmas with parallel current profile control. The sawtooth cycle disappears. Electron thermal diffusion is low (~5–10 m^2/s), the global energy confinement time increases and the core electron temperature increases fourfold,[23–25] in this case. Electron temperature fluctuations

associated with tearing modes are reduced to ~2% of the mean temperature, compared to 5%–30% in standard plasmas (See Fig. 12). No clear electron temperature structure is associated with these modes.

V. DISCUSSION

Burst mode Thomson scattering diagnostic capabilities have enabled the study of electron thermal characteristics of magnetic islands. In standard plasmas two different results have been observed: a temperature flattening across a $m=1$, $n=6$ magnetic island between sawtooth crashes and a helically peaked temperature profile inside the separatrix of a $m=1$, $n=5$ magnetic island after the sawtooth crash. The presence of a helically peaked postsawtooth temperature profile has not been reported before in MST plasmas. Its presence indicates a transient region of improved confinement that is in sharp contrast to the conventional view that RFPs are completely dominated by stochastic transport after the sawtooth crash. This result may have physics in common with the single helical axis (SHAx) structure and associated improved confinement observed in modified reversed field experiment (RFX-mod).[11] Note that the amplitude of the $m=1$, $n=5$ mode does not dominate the magnetic spectrum, therefore it is not identical to the SHAx state in RFX-mod.

For the $m=1$, $n=6$ mode the difference in the slope of the temperature profile across the X-point and O-point for the mode show that transport is significantly increased within the separatricies of the tearing mode relative to the background. In the case of the $m=1$, $n=5$ mode the opposite is observed with the presence of a temperature peaking. Local power balance calculations near the $m=1$, $n=5$ mode can be used to estimate the local thermal diffusion within the helical temperature structure. The power balance equation is

$$\frac{3}{2}\frac{\partial}{\partial t}(p_e) = S - \frac{1}{\rho}\frac{\partial}{\partial \rho}(\rho Q_e), \tag{11}$$

where the electron pressure, $p_e=n_eT_e$. The peak in electron temperature defines the flux surface coordinate $\rho=0$. The coordinate ρ represents an appropriate "radial-like" label relative to the center of the helically rotating structure. The quantity S describes sources and sinks. The heat flux, Q_e is modeled in terms of the electron thermal diffusivity

$$Q_e = -\chi_e n_e \nabla_\rho T_e. \tag{12}$$

Rearranging Eq. (12) to solve for χ_e provides the appropriate relation

$$\chi_e = \frac{\frac{1}{\rho}\int\left[\frac{\partial}{\partial t}\left(\frac{3}{2}n_eT_e\right) - S\right]\rho d\rho}{n\nabla_\rho T_e}. \tag{13}$$

Assuming the only source is the Ohmic power, ηJ^2, and that n_e, η and J are constant (n_e has not been measured and it may also fluctuate) in the small region near the helical temperature peak

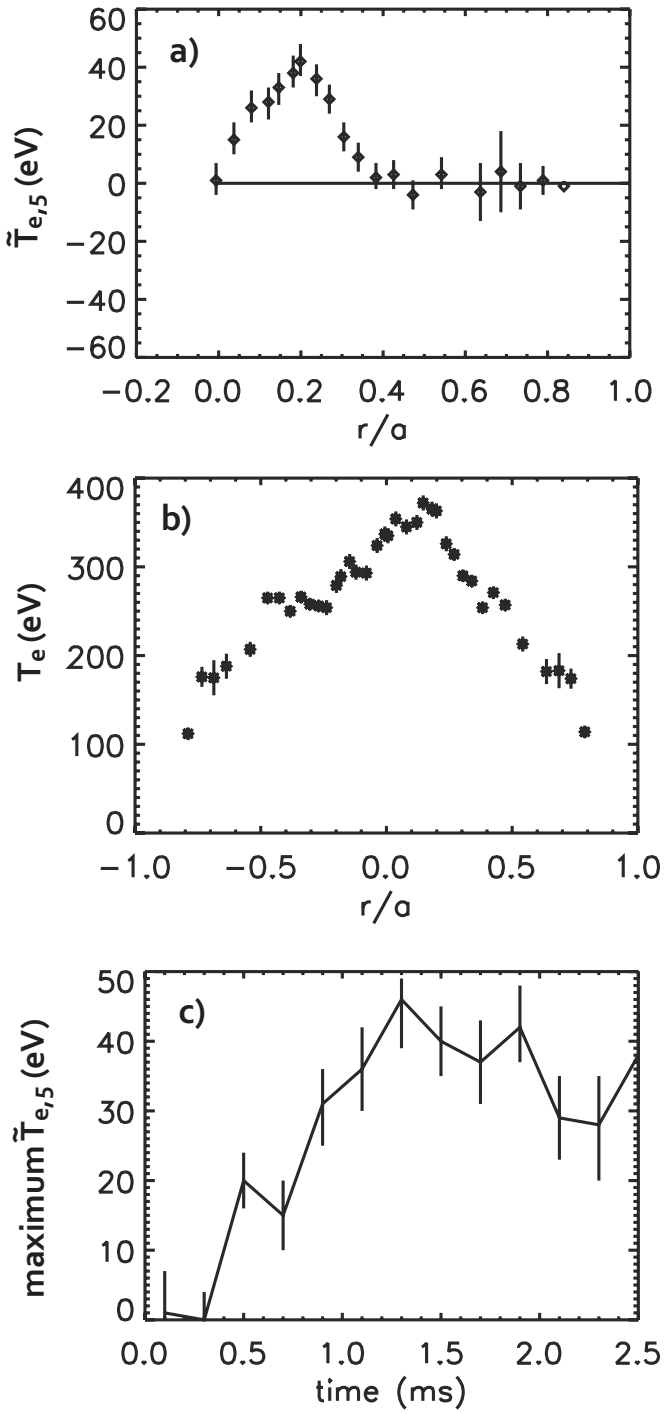

FIG. 10. (a) Electron temperature fluctuation amplitude associated with the $m=1$, $n=5$ tearing mode at $t=1.9$ ms after the sawtooth crash. (b) Combining mean temperature and fluctuation amplitude results, the electron temperature is plotted across a X-point (left side) and across an O-point (right side) showing an off-axis temperature peak with a helical $m=1$, $n=5$ characteristic. (c) The maximum fluctuation amplitude grows after the sawtooth crash and peaks at $t\sim1.3$ ms.

$$\chi_e = \frac{3n_e\int\frac{\partial T_e}{\partial t}\rho d\rho - \rho^2\eta J^2}{2n_e\rho\frac{\partial T_e}{\partial \rho}}. \tag{14}$$

The electron thermal diffusivity near the $m=1$, $n=5$ mode is shown in Fig. 13. Before the associated temperature structure

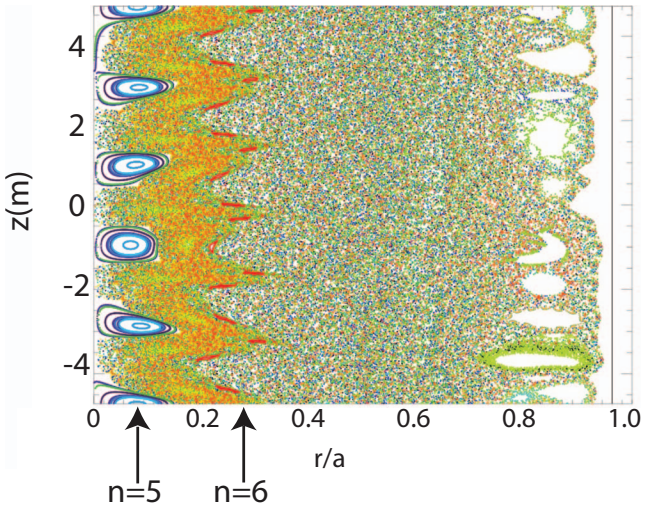

FIG. 11. (Color) Field line puncture plot from resistive MHD simulations shows intact flux surfaces inside the $m=1$, $n=5$ island after a sawtooth crash.

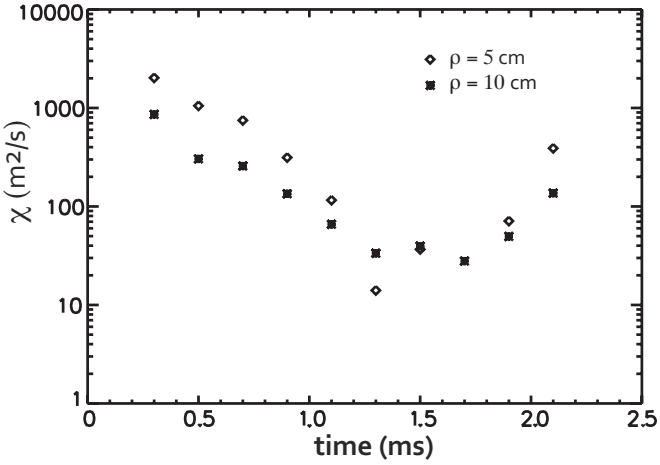

FIG. 13. Electron thermal diffusivity near the $m=1$, $n=5$ magnetic mode, $\rho=5$ cm($\sim 0.1\ r/a$) and $\rho=10$ cm($\sim 0.2\ r/a$).

appears χ_e is high (1000 m^2/s). As the temperature peak appears χ_e drops, reaching 30 m^2/s at its lowest, one to two orders of magnitude lower than a stochastic field and approaching that in improved confinement plasmas discussed in Sec. IV C.

The reason for the different characteristics associated with the $m=1$, $n=6$ and $m=1$, $n=5$ modes is unclear. The $m=1$, $n=6$ mode is always resonant in the core of the plasma. It is somewhat spatially isolated (not completely overlapping) from its nearest neighboring resonant tearing mode and spatially separated from the magnetic axis. The $m=1$, $n=5$ mode, however is not resonant before the sawtooth crash. It briefly may come into resonance at the sawtooth crash and is present for 2–4 ms afterward. MHD equilibrium reconstructions assuming axisymmetry show that $q(0)$ jumps up during the sawtooth crash and the $m=1$, $n=5$ mode becomes resonant very near the geometric axis. In this case the $n=5$ mode unlike the $n=6$ mode would have a resonant surface very close to the axis perhaps preventing a proper island structure from forming. However axisymmetric calculations of the equilibrium may not be sufficient to describe a plasma with a large helical temperature structure and it may be the case that the $n=5$ mode is not resonant. This supports the idea that the $n=5$ produces an ideal kinklike magnetic surface disturbance and not a tearing mode. 3D resistive MHD simulations show magnetic flux surfaces intact inside of an $m=1$, $n=5$ magnetic structure after the crash in contrast to flux surfaces which have been washed out inside of an $m=1$, $n=6$ island before the crash. Such a $m=1$, $n=5$ structure is superficially similar to the SHAx structure observed in the RFX-mod.[11] However, in MST the $n=5$ mode does not dominate the spectrum, and is only slightly larger than the next largest mode ($n=6$) immediately after the sawtooth crash in MST. This is in marked contrast to the SHAx structure in which a single mode dominates the spectrum. There is some similarity to SHAx operation as confinement in the vicinity of the postsawtooth crash $m/n=1/5$ structure is substantially improved.

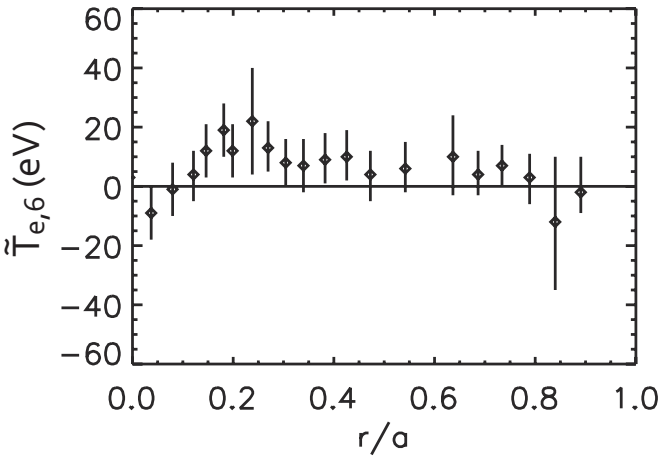

FIG. 12. Electron fluctuations (in a background of ~1300 eV) associated with small ($m=1, n=6$) magnetic fluctuations during plasmas where inductive parallel current profile control is applied.

Electron thermal diffusion in the core of MST is low just after a sawtooth and slightly higher than when inductive parallel current profile control is applied. In the latter case tearing mode amplitudes are kept small and associated electron temperature fluctuations are also small. There is no discernible electron temperature fluctuation associated with these modes. This supports the idea that the magnetic fluctuations are small enough so that magnetic islands are not forming or that if magnetic islands are forming the gradient in the mean temperature is not great enough to provide a discernible flattening or peaking across these islands.

ACKNOWLEDGMENTS

The authors would like to thank Jack Amubel, Adam Beardsley, Mike Borchardt, Adam Falkowski, Don Holly, Cale Kasten, Rob O'Connell, Eli Parke, Phil Robl, Rebecca Shapiro, and Ming Yang for their work with the Thomson scattering diagnostic and Dalton Schnack, Ben Hudson, and Fatima Ebrahimi for their work with the DEBS and MAL codes.

This work is supported by U.S. Department of Energy

(Cooperative Agreement DE-FC02–05ER54814) and the National Science Foundation (Cooperative Agreement PHY-0821899). This research was performed under an appointment to the Fusion Energy Sciences Fellowship Program administered by the Oak Ridge Institute for Science and Education under Contract No. DE-AC05-06OR23100 between the Department of Energy and the Oak Ridge Associated Universities.

[1]R. N. Dexter, D. W. Kerst, T. W. Lovell, S. C. Prager, and J. C. Sprott, Fusion Technol. **19**, 131 (1991).
[2]H. P. Furth, J. Killeen, and M. N. Rosenbluth, Phys. Fluids **6**, 459 (1963).
[3]T. M. Biewer, C. B. Forest, J. K. Anderson, G. Fiksel, B. Hudson, S. C. Prager, J. S. Sarff, J. C. Wright, D. L. Brower, W. X. Ding, and S. D. Terry, Phys. Rev. Lett. **91**, 045004 (2003).
[4]W VII-A Team and R. Jaenicke, Nucl. Fusion **28**, 1737 (1988).
[5]Z. Chang and J. D. Callen, Nucl. Fusion **30**, 219 (1990).
[6]M. F. F. Nave, A. W. Edwards, K. Hirsch, M. Hugon, A. Jacchia, E. Lazzaro, H. Salzmann, and P. Smeulders, Nucl. Fusion **32**, 825 (1992).
[7]R. Fitzpatrick, Phys. Plasmas **2**, 825 (1995).
[8]C. C. Hegna and J. D. Callen, Phys. Fluids B **4**, 4072 (1992).
[9]M. N. A. Beurskens, C. J. Barth, N. J. Lopes Cardozo, and H. J. van der Meiden, Plasma Phys. Controlled Fusion **41**, 1321 (1999).
[10]R. Lorenzini, D. Terranova, A. Alfier, P. Innocente, E. Martines, R. Pasqualotto, and P. Zanca, Phys. Rev. Lett. **101**, 025005 (2008).
[11]RFX-mod Team and Collaborators, R. Lorenzini, E. Martines, P. Piovesan, D. Terranova, P. Zanca, M. Zuin, A. Alfier, D. Bonfiglio, F. Bonomo, A. Canton, S. Cappello, L. Carraro, R. Cavazzana, D.F. Escande, A. Fassina, P. Franz, M. Gobbin, P. Innocente, L. Marrelli, R. Pasqualotto, M.E. Puiatti, M. Spolaore, M. Valisa, N. Vianello, and P. Martin, Nat. Physics **5**, 570 (2009).
[12]S. Hokin, A. Almagri, S. Assadi, J. Beckstead, G. Chartas, N. Crocker, M. Cudzinovic, D. Den Hartog, R. Dexter, D. Holly, S. Prager, T. Rempel, J. Sarff, E. Scime, W. Shen, C. Spragins, C. Sprott, G. Starr, M. Stoneking, and C. Watts, Phys. Fluids B **3**, 2241 (1991).
[13]J. K. Anderson, C. B. Forest, T. M. Biewer, J. S. Sarff, and J. C. Wright, Nucl. Fusion **44**, 162 (2004).
[14]D. D. Schnack, D. C. Barnes, Z. Mikic, Douglas S. Harned, and E. J. Caramana, J. Comput. Phys. **70**, 330 (1987).
[15]B. Hudson, Ph.D. thesis, University of Wisconsin-Madison, 2006.
[16]J. A. Reusch, M. T. Borchardt, D. J. Den Hartog, A. F. Falkowski, D. J. Holly, R. O'Connel, and H. D. Stephens, Rev. Sci. Instrum. **79**, 10E733 (2008).
[17]H. D. Stephens, M. T. Borchardt, D. J. Den Hartog, A. F. Falkowski, D. J. Holly, R. O'Connell, and J. A. Reusch, Rev. Sci. Instrum. **79**, 10E734 (2008).
[18]R. O'Connell, D. J. Den Hartog, M. T. Borchardt, D. J. Holly, J. A. Reusch, and H. D. Stephens, Rev Sci Instrum. **79**, 10E735 (2008).
[19]D. J. Den Hartog, J. R. Ambuel, M. T. Borchardt, J. A. Reusch, P. E. Robl, and Y. M. Yang, "Pulse-burst operation of standard Nd:YAG lasers," J. Phys.: Conf. Ser. (to be published).
[20]D. Sivia, *Data Analysis: A Bayesian Tutorial* (Oxford University Press, New York, 2002).
[21]S. D. Terry, D. L. Brower, W. X. Ding, J. K. Anderson, T. M. Biewer, B. E. Chapman, D. Craig, C. B. Forest, R. O'Connell, S. C. Prager, and J. S. Sarff, Phys. Plasmas **11**, 1079 (2004).
[22]J. S. Sarff, S. A. Hokin, H. Ji, S. C. Prager, and C. R. Sovinec, Phys. Rev. Lett. **72**, 3670 (1994).
[23]M. R. Stoneking, N. E. Lanier, S. C. Prager, J. S. Sarff, and D. Sinitsyn, Phys. Plasmas **4**, 1632 (1997).
[24]J. S. Sarff, N. E. Lanier, S. C. Prager, and M. R. Stoneking, Phys. Rev. Lett. **78**, 62 (1997).
[25]B. E. Chapman, A. F. Almagri, J. K. Anderson, T. M. Biewer, P. K. Chattopadhyay, C.-S. Chiang, D. Craig, D. J. Den Hartog, G. Fiksel, C. B. Forest, A. K. Hansen, D. Holly, N. E. Lanier, R. O'Connell, S. C. Prager, J. C. Reardon, J. S. Sarff, M. D. Wyman, D. L. Brower, W. X. Ding, Y. Jiang, S. D. Terry, P. Franz, L. Marrelli, and P. Martin, Phys. Plasmas **9**, 2061 (2002).